

Query-Efficient Video Adversarial Attack with Stylized Logo

Duoxun Tang[†], Yuxin Cao[†], Xi Xiao^{*}, Derui Wang, Sheng Wen and Tianqing Zhu



Abstract—Video classification systems based on Deep Neural Networks (DNNs) have demonstrated excellent performance in accurately verifying video content. However, recent studies have shown that DNNs are highly vulnerable to adversarial examples. Therefore, a deep understanding of adversarial attacks can better respond to emergency situations. In order to improve attack performance, many style-transfer-based attacks and patch-based attacks have been proposed. However, the global perturbation of the former will bring unnatural global color, while the latter is difficult to achieve success in targeted attacks due to the limited perturbation space. Moreover, compared to a plethora of methods targeting image classifiers, video adversarial attacks are still not that popular. Therefore, to generate adversarial examples with a low budget and to provide them with a higher verisimilitude, we propose a novel black-box video attack framework, called Stylized Logo Attack (**SLA**). **SLA** is conducted through three steps. The first step involves building a style references set for logos, which can not only make the generated examples more natural, but also carry more target class features in the targeted attacks. Then, reinforcement learning (RL) is employed to determine the style reference and position parameters of the logo within the video, which ensures that the stylized logo is placed in the video with optimal attributes. Finally, perturbation optimization is designed to optimize perturbations to improve the fooling rate in a step-by-step manner. Sufficient experimental results indicate that, **SLA** can achieve better performance than state-of-the-art methods and still maintain good deception effects when facing various defense methods. We believe that the proposed **SLA** can raise awareness among the security community about the reliability and security of video classification systems and serve as a memorandum of possible attack methods for the future.

Index Terms—Video adversarial attacks, style transfer, video recognition systems

1 INTRODUCTION

VIDEO understanding tasks using DNN-based models can be seen everywhere, such as video action recognition [1], video object detection [2], and video segmentation [3]. At the specific application level, these models have also been widely applied

in fields such as autonomous driving [4], industrial vision [5], and medical science [6]. However, studies a decade ago indicated that DNNs are highly susceptible to adversarial attacks [7]–[9], which poses security issues when applied in real-world applications. Furthermore, as one of the most common media for information dissemination in today’s society, video’s convenient information dissemination conditions also bring security risks of exposing harmful information, which involves violence, pornography, hatred, terrorism, false information, etc., which will threaten the physical and mental health of minors, and cause politically sensitive controversies, public panic, or other consequences. And an attacker can maliciously manipulate pixels in illegal videos to achieve that. Thus, equal attention must be given to attack methods as a means to gain a better understanding of adversarial attacks, in order to prepare adequately for potential future attacks. In recent years, designing attack methods from the perspective of attackers has become a widely researched area [10]–[17], aiming to draw attention from the security community and simulate potential future attacks.

From the external manifestations of attacks, existing types of unrestricted attacks can be roughly divided into two categories: style-transfer-based attacks [15], [18] and patch-based attacks [10], [14]. Specifically, both types of attacks involve superimposing a finely designed perturbation (global or local) on a clean sample to induce the classifier to make incorrect judgments. In extreme cases, modifying only one pixel of a clean sample can achieve the attack. For style-transfer-based attacks, their capability to alter all pixels can render the overall style of the sample unnatural. Compared to style-transfer-based attacks, patch-based attacks are regarded as perturbations that are more applicable to the real physical world. They introduce perceptible but local changes in sub-regions. For example, constraining the perturbations to an ℓ_p ball can limit the perceptibility of the perturbations. However, existing research has shown that such constrained attacks can be defended against by adversarial defenses. Perturbation constraints are unnecessary for patch-based attacks since their region is already limited. However, it is precisely because patch-based attacks perturb only small sub-regions that a current limitation of this attack family is its poor performance in targeted attacks [11]–[13]. This prompts attackers to consider how to approach the decision boundary of the classifier use such sub-regions.

Some white-box setting attacks [19]–[22], due to their access to more model information, precise gradient information, and accurate perturbation optimization, have achieved very successful results. However, real-world attackers often have no access to the structure and parameters of the target model, operating under

[†] Duoxun Tang and Yuxin Cao contributed equally to this paper.

^{*}Xi Xiao is the corresponding author.

Duoxun Tang is with the College of Science, Sichuan Agricultural University, Ya’an, China. Email: duoxuntang@stu.sicau.edu.cn. Yuxin Cao is with the School of Computing, National University of Singapore, Singapore. Email: yuxincao@comp.nus.edu.sg. Xi Xiao is with the Tsinghua Shenzhen International Graduate School, Tsinghua University, Shenzhen, China. Email: xiaox@sz.tsinghua.edu.cn. Derui Wang is with the Cyber-security and Quantum Systems Group, CSIRO’s Data61, Australia. Email: derek.wang@data61.csiro.au. Sheng Wen is with the School of Science, Computing and Engineering Technologies, Swinburne University of Technology, Melbourne, VIC, Australia. Email: swen@swin.edu.au. Tianqing Zhu is with the Faculty of Data Science, City University of Macau. Email: tqzhu@cityu.edu.mo.

stricter information acquisition assumptions such as label-only [23]–[27] or score-based [28]–[32], as attacks are typically initiated externally. One significant drawback of many current black-box setting attacks compared to white-box setting attacks is that the former often require a large number of queries to find adversarial examples. Additionally, patch-based attacks exacerbate this issue in the black-box setting when conducting targeted attacks. Therefore, considering the weak targeted attacks effectiveness of patch-based attacks and the query-unfriendly nature of black-box settings, designing an adversarial patch that can efficiently launch targeted attacks in a black-box setting presents a major challenge for attackers.

To address the challenges mentioned above from the attacker’s perspective, we propose a brand new attack framework called Stylized Logo Attack (**SLA**) against video classification systems based on stylized patch. Operating within a black-box setting, **SLA** combines the strengths of style-transfer-based and patch-based attacks, forming a style-transfer-based patch attacks that is efficient in queries and demonstrates satisfactory success rates on both targeted and untargeted attacks. Unlike existing stylized attacks that perturb entire videos globally, **SLA** perturbs only sub-regions of the video and stylizes these sub-regions to carry more target-class features, thus approaching or even surpassing the decision boundary of the classifier to compensate for the shortcomings of patch-based attacks in targeted attacks. Specifically, our attack consists of three main steps. Firstly, we construct a style set S_s by randomly initializing style reference images and introduce a logo set S_l as candidate patch types. Logos are chosen due to their inherent basic semantics, making them less perceptible. Secondly, we employ reinforcement learning to search for the optimal attributes of the Logo (pattern, style, and position parameters) and overlay the stylized logo onto appropriate positions in the clean video to create an adversarial example. The optimization of the optimal Logo attributes search is guided by a reward function specifically designed by us, considering confidence scores, Logo size, and coordinates to maximize perturbation effectiveness while enhancing overall visual naturalness. Lastly, we include a perturbation optimization stage based on random search to mitigate the weakness of existing Patch-based/RL-based methods in search space inadequacy. In extensive comparative experiments conducted on three mainstream datasets (UCF-101 [33], HMDB-51 [34] and Kinetics-400 [35]) against existing patch-based attacks, **SLA** demonstrates good performance in both targeted and untargeted attacks, with generated adversarial videos retaining semantic integrity. We also evaluate the robustness of **SLA** against defense scenarios.

This paper builds upon our earlier conference paper [36]. The new contributions it presents are outlined below:

- We introduce an innovative stylized patch-based attack framework, termed **SLA**, which employs a random search strategy for perturbation execution. This framework accomplishes attacks by superimposing extra stylistic attributes onto patches within clean videos. It allows perturbations to closely approach decision boundaries through stylization, while remaining imperceptible in localized sub-regions.
- We utilize RL to search for the optimal way to overlay patches, defining a new search space for patch attributes. Correspondingly, we design a specific reward function that considers the impact of patch size and position on the semantic information loss introduced to the video.
- We supplement a perturbation optimization stage that utilizes

square-shaped random search after RL to overcome the limited effectiveness of patch-based attacks in targeted scenarios and the restricted search space of RL, which can ensure the feasibility of targeted attacks in **SLA**.

- Besides UCF-101 and HMDB-51, we extend **SLA** to a larger dataset, Kinetics-400. Our approach outperforms state-of-the-art methods in representative metrics. Additionally, it exhibited optimal robustness when faced with different patch-based defense methods.
- This paper provide more comprehensive attack examples across various methods in different scenarios, and add two sets of user studies to verify imperceptibility of the adversarial videos generated by **SLA**.

The remaining sections of this paper are organized as follows: An overview of related work is provided in Section 2. Section 3 explains the preliminary information. Section 4 details the proposed solution. Section 5 outlines the experimental setup and presents the validation results. Finally, Section 6 summarizes the paper and provides prospects for future work.

2 RELATED WORK

In this section, an overview of existing restricted attacks related to our research is presented. Subsequently, two predominant types of attacks within the realm of unrestricted attacks are introduced. Defenses against patch-based attacks are depicted at last.

2.1 Restricted Attacks

To ensure the imperceptibility of perturbations, many works [37]–[41] focus on generating adversarial video x_{adv} from clean video x to fool the DNN-based models, while keeping x_{adv} within the ϵ_{adv} -ball of x ($\|x_{adv} - x\|_p \leq \epsilon_{adv}$). Some white-box setting attacks [8], [42], [43] have the access to the specific structure of the victim models, adversary can get more precise information such as gradient. Influenced by real-world scenarios, the black-box setting has become the main research topic. Following the black-box setting, Jiang *et al.* [37] proposed the pioneering work for video attack (V-BAD), which utilizes tentative perturbations and partition-based rectifications. To overcome the expensive computation of dense attacks and further enhance the invisibility of perturbations, Wei *et al.* [38] proposed a sparse attack for video recognition models, which heuristically searches a subset of frames. With the development of RL, some attacks [44]–[47] incorporate RL to search the key regions or key frames of the video. However, due to the query-consuming or low-efficiency in targeted attack, these methods still have a considerable distance to go from practical application.

2.2 Style-transfer-based Attacks

Style transfer techniques [48], [49] facilitate the development of style-transfer-based attacks. Style-transfer-based attacks first emerged in the image domain, with AdvCam [18] being one representative example. Under constraints such as style loss, content loss, temporal loss [50] and smoothness loss [51] (*e.g.*, achieved through total variance loss as a form of regularization), adversarial examples are crafted to resemble legitimate natural styles. However, for videos, style-transfer-based attacks typically need to balance the content and style of stylized video while considering consistency between frames [52].

StyleFool [15] was the first to utilize style-transfer-based attacks for videos without restrictions, incorporating temporal loss in addition to the classic constraints mentioned above. It also introduced style references carrying target class features to approximate the decision boundary of the target class, achieving notable success in targeted attacks. However, a common drawback of style-transfer-based attacks is that global perturbations may inevitably result in unrealistic object colors and decrease the naturalness of adversarial videos.

2.3 Patch-based Attacks

The typical characteristic of a patch-based attack [10], [10], [11], [13], [14] is the addition of perceptible patches to local areas of clean examples, which effectively mislead classifier systems without introducing the global unnaturalness often associated with style transfer. Initially, naïve approaches to such attacks, like HPA [53], used solid-color patches for perturbations, but proved ineffective for targeted attacks. Research indicated that CNNs are particularly sensitive to striped perturbations [54], also a detail leveraged by Square-Attack (SA) [32]. SA initializes clean images with vertical stripes before conducting a random search for square-shaped perturbations.

The attributes of patches can be structured into a search space, leading patch-based attacks to frequently employ RL for optimization. Specifically, given a search space, RL utilizes an agent to execute policies and adjust/improve them based on environmental feedback. In RL-based attacks, the attributes (position, shape, transparency, size, reference, etc.) of the adversarial patch are defined as the search space required by RL, making the attack process a decision-making process for the agent. The rise of RL-based attacks in adversarial attack-defense tasks is significant because RL transforms perturbations into an optimization problem rather than random search, thus enhancing attack efficiency. Several representative attack frameworks have been proposed. For example, PatchAttack [10] is used to attack images and achieves over 99% success rate in untargted attacks on ImageNet [55], but only a 10% success rate in targeted attacks. Moreover, many real-world patterns (such as bullet comments, watermarks, logos, etc.) have practical semantics, allowing patch-based attacks to utilize these patterns for more natural semantic information. For example, both BSC [13] and adv-watermark [11] utilize semantic patches for attack purposes. However, due to issues with patch transparency, the effectiveness of adv-watermark attacks is sometimes compromised. BSC achieves natural and inconspicuous effects by adding common bullet comments, but its effectiveness in targeted attacks remains limited.

Furthermore, many real-world scenarios can be viewed as gradient-free optimization problems, enabling attacks based on evolutionary algorithms (EA), such as STDE [56]. STDE aims to minimize the patch and utilizes spatial-temporal mutation and crossover to search for the global optimum.

The main reason some of these methods fall short in targeted attacks is the limited search space of RL and the neglect of further optimization for applied perturbations. This makes patch-based attacks challenging to succeed in targeted attacks, especially in videos where the additional time dimension complicates single-round perturbations.

2.4 Defense against Patch-based Attacks

Some research from the defender’s perspective has proposed various defense methods. With the emergence of adversarial

examples, a direct and classical idea is to train classifiers by mixing adversarial examples and clean samples to enhance the robustness of the classifier. However, the effectiveness of this defense mechanism may depend on whether the perturbations are constrained, and it may not perform well against attacks with unrestricted perturbations. For patch-based attacks, some specialized methods have been proposed. Among them, Local Gradient Smoothing (LGS) [57] suppresses those high activation regions by estimating noise locations in the gradient domain and regularizing their gradients. Patch Cleanser (PC) [58] restores benign predictions through a two-round mask approach. Additionally, due to the regional nature of patches, some object detection methods in computer vision (CV) have been proposed to detect attacked regions. For example, PatchZero [59] repairs adversarial examples by filling patch regions with zeros to make malicious patches benign. However, this method mainly faces two issues: the accuracy of patch position detection and the uncertain effectiveness of patch filling, which may even result in new adversarial examples. A good attack method should possess strong robustness against different defense mechanisms.

3 PRELIMINARY

In this section, the preliminary information is explained from three aspects. First, existing DNN-based video classifiers are introduced, followed by the definition of video adversarial attacks. Lastly, the threat model is depicted to manifest the attack scenarios and capabilities.

3.1 DNN-based Video Classifier

Many existing video classification systems in industry are predominantly DNNs with convolutional neural networks (CNNs) serving as the foundational feature filters. For a classifier, it recognizes patterns within a video containing complex semantics and provides corresponding behavioral class labels along with confidence scores. Several representative video classifiers such as TSN [60], C3D [61], Non-local (NL) [62], TPN [63], and I3D [64] have demonstrated excellent performance in video recognition tasks. Specifically, TSN segments the entire video and samples it to enable the network to process longer-duration videos, thereby extracting more temporal features. C3D implements fast inference and efficient computation based on simple 3D ConvNets, making it well-suited for widespread industrial deployment. NL captures long-range dependencies among video features through non-local operations. TPN focuses on modeling visual tempos of video actions. I3D learns seamless spatio-temporal features using two-stream Inflated 3D ConvNets. Among these models, since C3D [61] and two-stream networks like I3D [64] possessing representativeness and compatibility, C3D and I3D are considered as victim models in this paper.

3.2 Problem Definition

Given a classifier f , its objective is to receive a clean video $x \in \mathbb{R}^{T \times C \times W \times H}$ and classify it, where T , C , W , and H represent the frame number, channel number, width, and height of the clean video, respectively. The attacker’s objective is to cause the classifier f to misclassify. Following a black-box setting, the attacker can only access its top-1 predict label y and its score $p(y|x)$. Then, given an attack A , we can obtain adversarial examples $x_{adv} = A(x)$. The attacker has two types of attack objectives: targeted

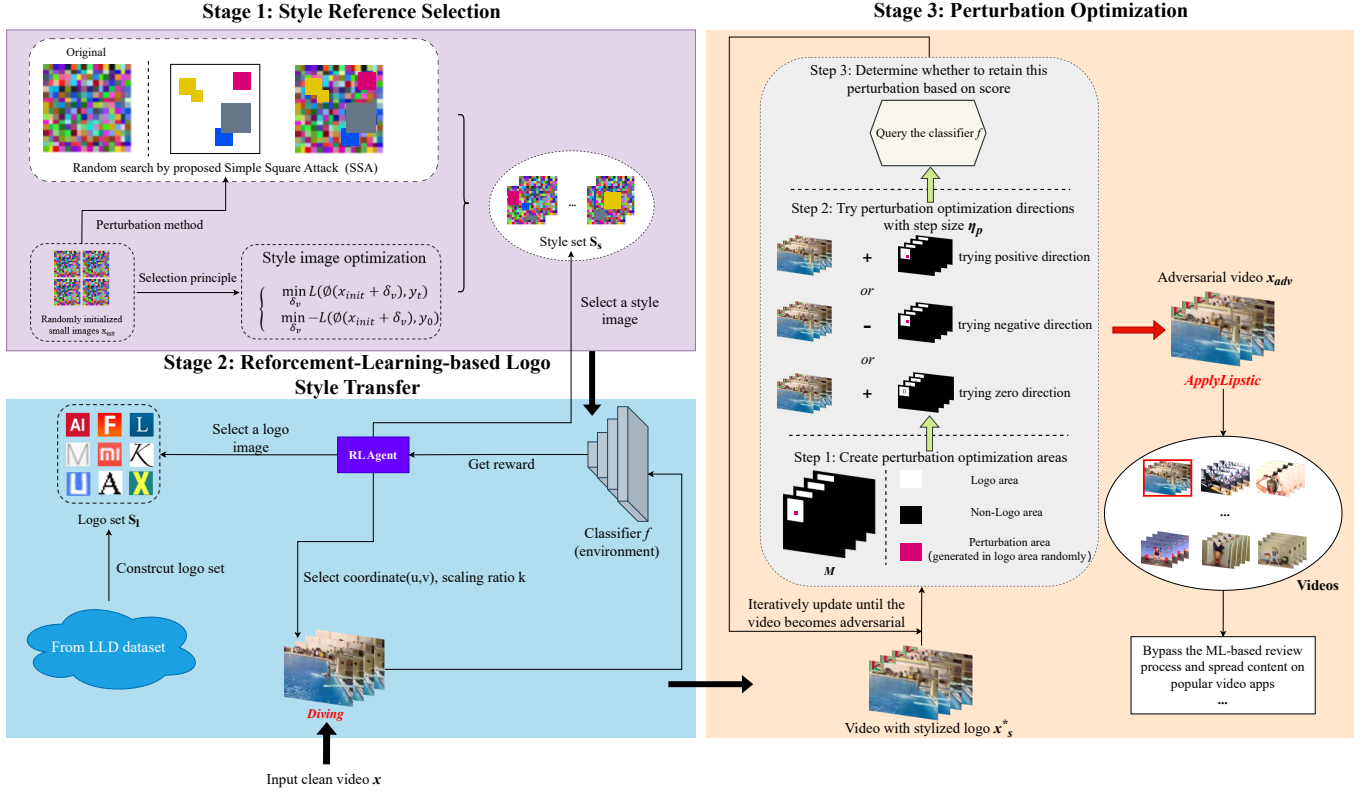


Fig. 1: Architecture of SLA.

attack, where the goal is to fool f such that $f(x_{adv}) = y_t$, and untargeted attack, where the objective is to make $f(x_{adv}) \neq y_0$. Here, y_t and y_0 respectively denote the target label and original true label of x . The adversary's goal can be represented by the following formula.

$$\begin{cases} f(x_{adv}) = y_t, & \text{if targeted,} \\ f(x_{adv}) \neq y_0, & \text{if untargeted.} \end{cases} \quad (1)$$

3.3 Threat Model

Attack Scenarios. SLA is applicable to the offline scenario (the adversary has access to the target videos and models on a local basis), and SLA only focuses on one-on-one attacks (the adversary generates the perturbations tailored to each individual input video) to superimpose stylized logo on a static clean video. Then the adversarial video will make the victim model output wrong prediction.

Attack Capabilities. In this research, the capabilities of adversary are listed as follows. Attacker can establish a suitable logo set from public datasets (e.g., LLD dataset [65]) for logo reference selection. Figure 2 shows some examples of logo reference. To more closely align with real attack scenarios, attacker follows the black-box setting. Specifically, given an adversarial video x_{adv} and a victim classifier f , adversary can only access the top-1 label y and its confidence score $f(y|x)$. Thus, SLA also can be regarded as a score-based attack. Furthermore, following the setting of previous works [15], [36], a maximum query limit is set to avoid meaningless queries if the algorithm is hard to converge, which is also close to the fact that the query costs are limited in practical scenarios.

4 METHOD

In this section, the details of the three main stages of SLA: Style Reference Selection, RL-based Logo Style Transfer, and Perturbation Optimization are described. The specific attack process of SLA is illustrated in Figure 1.

4.1 Style Reference Selection

The goal of this stage is to establish a style set that enables the stylized logo to carry more features about the target label in targeted attacks (other labels in untargeted attacks).

4.1.1 Purpose of Selection

To reduce computational complexity, we first initialize a small tensor $x_{init} \in \mathbb{R}^{C \times W_i \times H_i}$ following a uniform distribution as the candidate style reference tensor, where W_i and H_i represent the width and height of the initialized tensor respectively. For targeted attacks, we perform local pixel-level modifications on x_{init} using a patch-based unconstrained perturbation, aiming to make x_{init} carry more features of the target class. Let $x_v = x_{init} + \delta_v$, where δ_v represents the perturbation, such that $f(\phi(x_v)) = y_t$, where the symbol ϕ denotes the resizing function, which scales up the small, perturbed initialized tensor to match the dimensions of the original input video x , y_t denotes the target class label. This is because in subsequent attacks, the logo style-transferred by x_v is attached on the clean video, which moves the new video close to the decision boundary of the classifier f . For untargeted attacks, a suitable x_v only needs to ensure that the classification result after superimposing the perturbation δ_v is no longer the label y_0 of the original video, i.e., $f(\phi(x_v)) \neq y_0$. Therefore, the purpose of Style Reference Selection is to find appropriate perturbations δ_v^* to obtain a satisfactory style tensor denoted as $x_v^* = x_{init} + \delta_v^*$.

Algorithm 1: Style Reference Selection.

Input: Black-box classifier f , original label y_0 , target label y_t , perturbation iterations I , perturbation size coefficient α .

Output: Appropriate style image set S_s .

```

1  $i \leftarrow 0$ ;
2  $S_s \leftarrow []$ ;
3 while not meeting the termination condition do
4    $x_{init} \leftarrow \text{random\_init}()$ ;
5    $last\_score \leftarrow f(\phi(x_{init}))$  // replace  $y_t$  with  $y_0$  for
   untargeted;
6   for  $i < I$  do
7      $h \leftarrow \text{alpha\_schedule}(\alpha, i, I, H_i, W_i)$ ;
8      $(P_{\delta_u}, P_{\delta_v}) \leftarrow \text{random\_select}(h, H_i, W_i)$ ;
9      $\delta_v \leftarrow \text{generate\_perturbation}(P_{\delta_u}, P_{\delta_v}, h)$ ;
10     $temp \leftarrow x_{init}$ ;
11     $temp \leftarrow temp + \delta_v$ ;
12    if  $f(\phi(temp)) > last\_score$  // replace it with
     $f(\phi(temp)) < last\_score$  for untargeted then
13       $last\_score \leftarrow f(\phi(temp))$ ;
14       $x_{init} \leftarrow temp$ ;
15    else
16       $temp \leftarrow x_{init}$ ;
17       $temp \leftarrow temp - \delta_v$ ;
18      if  $f(\phi(temp)) > last\_score$  // replace it with
     $f(\phi(temp)) < last\_score$  for untargeted then
19         $last\_score \leftarrow f(\phi(temp))$ ;
20         $x_{init} \leftarrow temp$ ;
21    if  $f(\phi(x_{init})) = y_t$  // replace it with
     $f(\phi(x_{init})) \neq y_0$  for untargeted then
22       $x_v^* \leftarrow x_{init}$ ;
23       $S_s.append(x_v^*)$ ;
24      break;
25 return  $S_s$ .
```



Fig. 2: Some examples of logo references.

satisfying the aforementioned conditions. This constraint can be achieved using a simple cross-entropy loss:

$$\begin{cases} \min_{\delta_v} L_{CE}(\phi(x_{init} + \delta_v), y_t), & \text{targeted,} \\ \min_{\delta_v} -L_{CE}(\phi(x_{init} + \delta_v), y_0), & \text{untargeted,} \end{cases} \quad (2)$$

where L_{CE} is the cross-entropy loss.

4.1.2 Simple Square Attack

Inspired by both the Simple Black-box Attack (SimBA) [31] and Square Attack (SA) [32], we propose an improved version of SA, referred to as Simple Square Attack (SSA), which is also a score-based attack. Specifically, SSA aims to add multiple rounds of square-shaped perturbations to the x_{init} (perturbations added in the same round are identical). The square-shaped perturbations added by SSA mainly have two attributes: the length of the side of the squares and position (pixel coordinates of the top-left corner),

denoted as h and $(P_{\delta_u}, P_{\delta_v})$, respectively. For h , it given by the closest positive integer:

$$h = \text{round}(\sqrt{\alpha \times W_i \times H_i}), \quad (3)$$

where round represents the rounding operation and α is the coefficient determining the perturbation size. Its size follows a predefined piece-wise constant schedule and decreases segmentally with the number of perturbation iterations. For the position coordinates $(P_{\delta_u}, P_{\delta_v})$, SSA randomly selects two integers from the range $0 \sim (W_i - h)$ to assign to $(P_{\delta_u}, P_{\delta_v})$, where $(W_i - h)$ ensures that the selected pixel perturbation area does not exceed the boundaries of x_{init} . Once the attributes h and $(P_{\delta_u}, P_{\delta_v})$ are obtained, the perturbation in each round is a tensor with the shape $\delta_v \in \mathbb{R}^{C \times h \times h}$. The position of the square-shaped perturbation satisfies:

$$(P_{\delta_u}, P_{\delta_v}) = (\text{rs}(0, W_i - h) \cap \mathcal{Z}, \text{rs}(0, W_i - h) \cap \mathcal{Z}), \quad (4)$$

where rs represents randomly selecting pixel coordinates within a certain range. This implies the ability to sample any square subset of the input and add square-shaped perturbations. For the elements of the δ_v , they are initialized to a constant value. This pixel value of x_{init} will change in different directions influenced by δ_v , i.e., in each round, each pixel of x_{init} can only be altered by one of $\{-\eta, 0, \eta\}$ relative to its initial pixel, where η denotes the step size. Then, the perturbations that are beneficial for deception classifier f are retained.

To expand the search space for RL-based Logo Style Transfer in the second stage and to obtain more diverse stylized logo to resist defense, the aforementioned style reference selection will be performed N times to obtain a variety of style selections (constitute the style set S_s). The overall process of SSA in Style Reference Selection is depicted Algorithm 1. random_init represents the randomly initialization for small images, alpha_schedule is a predefined piece-wise constant schedule, and the output determines the perturbation size h . random_select represents the random selection of square-shaped perturbations. $\text{generate_perturbation}$ performs the perturbation generation operation. append adds the suitable style image to the style set S_s .

4.2 RL-based Logo Style Transfer

The aim of this stage is to obtain a stylized logo that has optimal attributes selected by RL and to superimpose it on the clean video.

4.2.1 Logo Style Transfer

Given the style image x_v , and given a pair consisting of a logo image l and its corresponding stylized logo l_s , the loss function includes three constraints as described below.

To enhance the semantic similarity between the original logo image l and its stylized counterpart l_s , the content loss is defined as:

$$L_{\text{content}}(l^i, l_s^i) = \sum_k \frac{1}{H_k W_k C_k} \|\vartheta_k(l^i) - \vartheta_k(l_s^i)\|_2^2, \quad (5)$$

where l^i represents the logo image superimposed on the i -th frame of the video, while l_s^i denotes the stylized logo on the same frame. H_k , W_k , and C_k represent the height, width, and number of channels of the feature maps at the k -th layer. ϑ signifies the feature extractor. The output of one layer of VGG-19 [66], which serves as the feature extractor, is utilized to calculate the content

loss. This approach not only achieves good conversion results but also reduces computational complexity. Moreover, a style loss is introduced to reduce the difference between l_s and x_v :

$$L_{\text{style}}(l_s^i, x_v) = \sum_k \frac{1}{C_k^2} \|G_k(x_v) - G_k(l_s^i)\|_2^2, \quad (6)$$

where G represents the Gram matrix in the k -th layer [51]. By introducing content loss and style loss, the goal is to enable the video with the stylized logo to approach or even surpass the classifier's decision boundary. Last, a total variance loss [51] is implemented to suppress noise, making the stylized tensor smoother and acting as a regularization term in the total loss:

$$L_{tv}(l_s^i) = \sum_{u,v} \left(\|l_s^i(u, v) - l_s^i(u+1, v)\|_2^2 + \|l_s^i(u, v) - l_s^i(u, v+1)\|_2^2 \right), \quad (7)$$

where (u, v) represents the pixel coordinates of stylized logo l_s .

Thus, the entire objective for Logo Style Transfer is:

$$l_s^* = \arg \min_{l_s} \lambda_c L_{\text{content}}(l, l_s) + \lambda_s L_{\text{style}}(l_s, x_v) + \lambda_{tv} L_{tv}(l_s), \quad (8)$$

where λ_c , λ_s , and λ_{tv} are the weights of each loss to control their respective effects.

4.2.2 Logo attribute selection

Selecting the right location, size, logo and style for the video is a crucial step for launching attacks, and it also helps to reduce the number of queries required in perturbation optimization stage. Specifically, considering several attributes of the logo in this task: the position of the logo in the video, the size of the logo, the pattern of the logo, and the style reference of the logo. These attributes determine the effectiveness of the attack. Combining these attributes forms the attribute space defined as the search space S for RL:

$$S = (u, v, k, l_{\text{ind}}, s_{\text{ind}}), \quad (9)$$

where u and v represent the pixel coordinates of the top-left corner of the logo in each frame of the video, k denotes the scaling factor for the size of the logo, l_{ind} stand for the index of the selected logo from the established logo set S_l , and s_{ind} signifies the index of the style reference selected from the style set S_s . Given a clean video x and the size of the logo as h and w , the range of pixel coordinates are determined as: $u \in [0, H - kh] \cap \mathbb{Z}$, $v \in [0, H - kh] \cap \mathbb{Z}$.

The training objective of the agent is to generate a suitable sequence of attack actions, which includes five action elements: the aforementioned u , v , k , l_{ind} , and s_{ind} . Once the agent is sufficiently trained, it can sample an optimal sequence of actions for superimposing logo on the clean video, resulting in a stylized logo that is scaled by a factor of k , with the logo style index being l_{ind} and the style reference index being s_{ind} , placed at position (u, v) in each frame of the video.

For the reward function during the search process, in order to minimize the impact on the video's core semantics, it is encouraged that the logo is positioned near the corners of the video and the size of logo is small. Most importantly, to make the video with the stylized logo approach or even surpass the classifier's decision boundary, confidence scores are incorporated into the reward function. This strategy is beneficial as it helps to reduce the number of queries needed in the next stage. In summary, three constraints are considered in constructing the reward function: logo

position, logo size and confidence scores. The reward function can be expressed as:

$$R = \begin{cases} \log p(y_t | x_s) - \mu_a k^2 h w - \mu_d d_m, & \text{targeted,} \\ \log(1 - p(y_0 | x_s)) - \mu_a k^2 h w - \mu_d d_m, & \text{untargeted,} \end{cases} \quad (10)$$

where x_s is the adversarial video with the stylized logo added, $k^2 h w$ actually calculates the area of the scaled stylized logo, and d_m is the distance from the four corners of the logo to the nearest corner in the video, *i.e.*,

$$d_m = \min\{d_{nw}, d_{ne}, d_{sw}, d_{se}\}, \quad (11)$$

among them, d_{nw} , d_{ne} , d_{sw} , and d_{se} represent the distances from the stylized logo to the four corners of the video, namely northwest, northeast, southwest, and southeast, respectively. μ_a and μ_d denote the penalty coefficients for the logo area and the distance mentioned above, respectively.

For the policy network, similar to previous work [10], [13], we choose an LSTM network that includes a fully connected layer. The action probability distribution given by the agent at time step t satisfies $p(a_t | (a_1, \dots, a_{t-1}))$, where a_t is sampled from Categorical function later. Subsequently, by using the Categorical probability, an action is sampled and its corresponding sampling probability is recorded. After traversing through all actions, the agent will generate a sequence of actions, as well as a sequence of probability π_{θ_p} corresponding to each action sampled at each step, where θ_p represents the parameters of the policy network. To minimize the distance between the action sampling distribution and the reward for the policy network, the loss function is defined as follows.

$$L(\theta_p) = -\mathbb{E}_{\tau \sim \pi_{\theta_p}} [R(\tau)], \quad (12)$$

the parameters of the policy network are updated using the approximate gradients obtained through multiple trajectory samplings [67], which can be expressed as:

$$\nabla_{\theta_p} L(\theta_p) \approx -\frac{1}{\Omega} \sum_{\tau=1}^{\Omega} \sum_{t=1}^{D_s} \nabla_{\theta_p} \log \pi_{\theta_p}(a_t | h_t) R(\tau), \quad (13)$$

where Ω and h_t respectively represent the number of sampling trajectories and the hidden state of the LSTM. By continuously optimizing the parameters θ_p of the policy function, the agent eventually obtains a sequence of actions that produce a logo with the best attributes, thereby achieving deception of the classifier. In this stage, the video x_s^* with the stylized logo is obtained.

Overall, stylized logos has three main benefits. 1) **Advantages for Attack Effects:** Stylized logos can carry more information of target classes in targeted attacks or that of classes other than original class in untargeted attacks, thereby moving videos with stylized logos close to or even across the decision boundary of the classifier f . 2) **Advantages against Defense Methods:** It is challenging for defense methods to detect patch-based perturbations that are located in unimportant positions and of small size. In addition, the diverse style images also create a variety of stylized logos, making adversarial defense methods hard to learn all the references of the stylized logo. 3) **Lower Human Alertness:** Human visual alertness tends to be less sensitive to small patches in the corners of the video.

4.3 Perturbation Optimization

To overcome the limitation of patch-based attacks, particularly in targeted attacks where the exploration space in RL is restricted, we

Algorithm 2: Stylized Logo Attack.

Input: Black-box classifier f , clean video x , original label y_0 , target label y_t , perturbation iterations I , perturbation size coefficient α in stage 1, search space S , step size η_p in stage 3, perturbation threshold ϵ in stage 3.

Output: Adversarial video x_{adv}

```

1  $S_s \leftarrow \text{style\_reference\_selection}(f, y_0, y_t, I, \alpha)$  //
  replace  $y_t$  with  $y_0$  for untargeted;
2 while not meeting the termination condition do
3    $a \leftarrow$  an action sequence  $(u, v, k, l_{ind}, s_{ind})$  sampled from
     $S$ ;
4    $x_v^* \leftarrow S_s(s_{ind})$ ;
5    $l_s^* \leftarrow \text{logo\_style\_transfer}(S_l(l_{ind}), x_v^*)$ ;
6    $M \leftarrow \text{cal\_mask}(u, v, k, x)$ ;
7    $x_s \leftarrow x + M \odot \text{pad}(l_s^*)$ ;
8   Calculate reward  $R$  for targeted/untargeted attacks;
9   Calculate RL loss gradient  $\nabla_{\theta_p} L(\theta_p)$ ;
10  Update policy network and the best video  $x_s^*$ ;
11  $x_{adv} \leftarrow \text{Logo-SSA}(f, x_s^*, y_t, u, v, \eta_p, \epsilon)$ . // replace  $y_t$  with  $y_0$ 
    for untargeted

```

introduce an additional stage to previously mentioned processes. This extension is termed as Logo-SSA. Logo-SSA focuses on perturbing the area where the logo is positioned. This approach expands the search space for patch-based attacks, which can increase the FR for targeted attacks.

Specifically, Perturbation Optimization uses random search to alter any pixel within the logo regions in a square-shaped manner. In each round, each pixel in logo regain can only be changed by one of $\{-\eta_p, 0, \eta_p\}$ compared to the original pixel. η_p signifies the optimization perturbation step size. The optimization process then proceeds as follows.

$$\min_{\delta_p} L_{CE}(x_s + M \odot \delta_p, y_t), \text{ s.t. } \|M \odot \delta_p\|_p \leq \epsilon, \quad (14)$$

where ϵ represents the perturbation threshold, δ_p denotes the perturbation, $M \in R^{T \times C \times W \times H}$ signifies the logo mask where the value in the logo region is 1, otherwise 0. Based on previous experimental attempts, the majority of videos cannot be turned into adversarial videos in just one round of attack, so the above optimization process will iterate through multiple rounds until success. In this stage, the optimization principles identical to those of Algorithm 1 are applied within the logo area.

4.4 SLA Recap

The overall process of SLA is shown in Algorithm 2, where `style_reference_selection` outputs the style set used for stylizing the logo, `logo_transfer` represents the style transfer process for stylizing the logo, `cal_mask` generates the corresponding-sized mask matrix based on the position, `pad` resizes the logo and places it in the correct position in each frame of the video, with pixels of the non-logo area filled with zeros. From Algorithm 2, the main workflow of SLA involves: constructing a suitable style set S_s , choosing the best attributes for the logo under the guidance of RL, and optimizing the perturbations of pixel values within the logo region.

5 EXPERIMENTAL EVALUATION

In this section, the experimental setup is initially introduced, encompassing a comprehensive overview of the datasets, target models,

benchmarks, and metrics. Subsequently, the preliminary experiments for the SLA are explained, focusing on the identification of key hyperparameters. The performance outcomes of various attacks are then presented. Additionally, a visualization is performed to illustrate the local regions that the victim model focuses on. An analysis of different attacks against defense mechanisms is also displayed. Finally, an ablation study is conducted to verify the effectiveness of the SLA.

5.1 Setup

5.1.1 Datasets

UCF-101 [33], HMDB-51 [34], and Kinetics-400 [35] datasets are chosen for conducting experiments. The UCF101 is an action recognition dataset featuring real-life action videos from YouTube, containing 13,320 videos in 101 action classes. HMDB-51, on the other hand, is a video database comprises 51 action categories, with approximately 7,000 manually annotated clips from various platforms, ranging from digital movies to videos on YouTube. Kinetics-400 is substantially larger, with two or more orders of magnitude of data. It consists of 400 human action classes, each class containing more than 400 segments extracted from realistic YouTube videos. In experiments, 100 videos are randomly selected from the test sets of each dataset to attack the target models. All selected videos are originally correctly classified by their respective classifiers. In addition, a logo set is constructed from the LLD dataset [65], which includes over 600,000 logos from around the world. Certain logos featuring an extensive array of transparent pixels may exhibit undesirable effects after style transfer, such as irregular coloration against a white backdrop, thereby diminishing the stealthiness of the stylized logos. Consequently, such logos are deemed incompatible with the style transfer process. To address this, data preprocessing is conducted on the LLD dataset by automatically removing logos with transparent pixels or a large number of white pixels, resulting in a suitable logo set denoted as S_l .

It is significant to note that Kinetics-400, with its larger number of classes and finer granularity, presents greater challenges for conducting targeted attacks on models leveraging this dataset. Results of attack performance in Section 5.3 also corroborate this observation.

5.1.2 Target Models

C3D [61] and I3D [64] are selected as target models for their distinct approaches to video analysis. C3D employs three-dimensional convolution to capture temporal features effectively, leading to robust classification accuracy. On the other hand, I3D focuses on the relationship between consecutive frames, leveraging optical flow to discern actions and achieving considerable classification performance.

For pretraining, C3D and I3D are trained on the training sets of UCF-101 [33] and HMDB-51 [34]. For Kinetics-400 [35], the weights provided by MXNet [68] are directly utilized. Due to differences in data processing, the input formats for C3D and I3D vary across UCF-101, HMDB-51, and Kinetics-400. Specifically, it is expected that the input format for I3D in Kinetics-400 is 32 frames, each with a size of 224×224 pixels, while other inputs consist of 16 frames, each with a size of 112×112 pixels. The video recognition accuracy for C3D and I3D on UCF-101 is 83.54% and 61.70%, respectively. For HMDB-51, the accuracy is 66.77% for C3D and 47.92% for I3D. On Kinetics-400, the accuracy is 59.5% for C3D and 71.8% for I3D.

5.1.3 Benchmarks

Five patch-based attacks, Sparse-RS [14], Adv-watermark [11], PatchAttack [10], BSC [13] and our conference work LogoStyle-Fool [36], are selected as benchmarks. PatchAttack is extended to videos and also considers rectangular patches with RGB perturbations to ensure fair comparison. Since BSC primarily focuses on untargeted attacks, it requires a slight adjustment to accommodate targeted attacks. Both benchmarks employ RL iteration for patch optimization, the iteration is stopped once the reward converges. However, success is not guaranteed, especially in targeted attacks. Due to the query constraints in our attack, the batch size and iteration steps are increased for both benchmarks to achieve relative fairness. Additionally, recognizing the similarity between watermarks and logos, Adv-watermark is also applied to video attacks, functioning as another. The default parameter values are maintained for the benchmarks. However, in BSC attacks, the feasibility of SLA’s third stage (perturbation optimization) is reduced due to varying bullet comment positions in video frames. Thus, for fair comparison, the results obtained through SLA without this stage are presented. In addition, the query limit is set as 3×10^5 akin to existing video attacks V-BAD [37] and StyleFool [15].

5.1.4 Metrics

The attack performance is evaluated by using the following metrics: 1) Fooling rate (FR). 2) Average query (AQ). 3) Average Occluded Area (AOA). 4) Temporal Inconsistency (TI). Specifically, their definitions are as follows.

Fooling rate (FR): this metric measures the proportion of adversarial videos that successfully mislead the classifier to either the target class (for targeted attacks) or any other class (for untargeted attacks) within the preset query limit.

Average query (AQ): AQ_1 , AQ_2 , and AQ_3 represent the average number of queries required in the first, second, and third stages, respectively. It’s worth noting that most targeted attacks require involvement in the third stage, which consumes the most queries. In contrast, untargeted attacks often succeed by the end of the second stage. Therefore, the success rate (2FR) and the number of queries required for success by the end of the second stage (2AQ) are also calculated to demonstrate the excellent performance of SLA without the need for perturbation optimization, especially in untargeted attacks.

Average Occluded Area (AOA): this metric evaluates whether logos/patches in videos significantly affect the core semantics of the videos or are perceptible by measuring their average occluded area in the videos.

Temporal Inconsistency (TI): TI is introduced to measure the temporal inconsistency of adversarial videos. Specifically, a warp function [50] is utilized to calculate the warping error E_{warp} , which is defined as follows.

$$E_{pair}(x_t, x_m) = \frac{1}{HWC} O_{t,s} \|x_t - \mathcal{W}(x_m)\|_1, \quad (15)$$

$$E_{warp}(x_t) = \frac{1}{T-1} \sum_{t=2}^T E_{pair}(x_t, x_1) + E_{pair}(x_t, x_{t-1}), \quad (16)$$

where $O_{t,m}$ denotes the occlusion mask matrix corresponding to the frames x_t and x_m . Meanwhile, the symbol \mathcal{W} signifies the operation of backward warping, which involves the utilization of optical flow to map pixels from one frame to another.

TABLE 1: Results of SLA with various style image number N_s .

N_s	UCF-101-Targeted					UCF-101-Untargeted				
	FR \uparrow	AQ $_1$	AQ $_2$	AQ $_3$	AQ \downarrow	FR \uparrow	AQ $_1$	AQ $_2$	AQ $_3$	AQ \downarrow
1	40%	337.6	1,758.2	8,158.9	10,254.7	100%	1.0	613.1	1,270.5	1,884.6
3	50%	1,474.3	1,800.4	7,114.7	10,389.4	100%	1.1	698.7	1,647.7	2,347.5
5	60%	1,556.1	1,798.5	5,001.2	8,355.8	100%	1.2	560.6	1,127.4	1,689.2
7	50%	1,646.2	1,615.8	6,891.4	10,153.4	100%	1.2	533.1	1,579.0	2,113.3
9	60%	2,585.3	1,732.3	8,011.4	12,329.0	100%	1.4	590.7	1,624.7	2,216.8
11	55%	3,158.1	1,795.2	9,044.5	13,997.8	100%	1.4	731.8	1,750.1	2,483.3

TABLE 2: Results of SLA with various logo number N_l .

N_l	UCF-101-Targeted					UCF-101-Untargeted				
	FR \uparrow	AQ $_1$	AQ $_2$	AQ $_3$	AQ \downarrow	FR \uparrow	AQ $_1$	AQ $_2$	AQ $_3$	AQ \downarrow
10	40%		1,662.1	13,533.5	17,033.0	100%		563.6	1,592.2	2,156.8
20	55%		1,705.4	12,681.2	16,780.0	100%		617.4	1,451.3	2,069.7
50	40%	1,899.8 \pm 382.7	1,683.0	17,290.5	21,102.1	100%	1.2 \pm 0.2	739.7	1,281.7	2,022.3
80	60%		1,688.4	11,293.6	14,590.5	100%		511.3	663.7	1,175.9
100	55%		1,702.3	14,039.6	16,995.6	100%		931.5	910.4	1,842.9
120	55%		1,858.8	16,092.8	20,128.6	100%		634.9	1,335.9	1,971.7

5.2 Hyperparameters Search

SLA has three important hyperparameters: style image number N_s , logo number N_l , and the step size η_p for optimizing perturbations in the third stage. Small-scale pre-experiments are conducted by randomly selecting 20 videos from UCF-101 to conduct both targeted and untargeted attacks against C3D. The grid search is used to find the optimal parameter combination.

The numerical results are analyzed from three aspects: 1) the impact of style image number N_s on AQ_1 , 2) the impact of logo number N_l on AQ_2 and 3) the impact of step size η_p on AQ_3 . Table 1 reports that larger N_s directly causes more queries (AQ_1) in style reference selection (Stage 1), but smaller N_s provides limited selection for the following stage, which may result in a narrow search space for RL. Moreover, excessive N_s results in the creation of redundant search space and hinders attack efficiency. Table 2 reveals that N_l tends to affect the convergence of queries (AQ_2) in RL-based logo style transfer (Stage 2). A valid reason is that sufficient N_l provides adequate search options for RL. Table 3 indicates that the step size η_p is an important hyperparameter that significantly impacts the total queries in a single attack, since the most query-consuming stage is perturbation optimization (Stage 3). A suitable step size η_p can overcome the dilemma of local optima caused by pulling the samples back onto the ℓ_{inf} ball. Therefore, the values of N_s , N_l , and η_p are finally set to 5, 80 and 0.2, respectively.

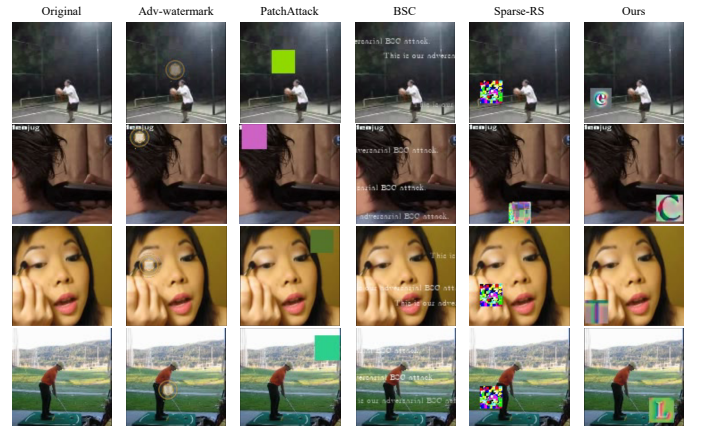


Fig. 3: Examples of different attacks.

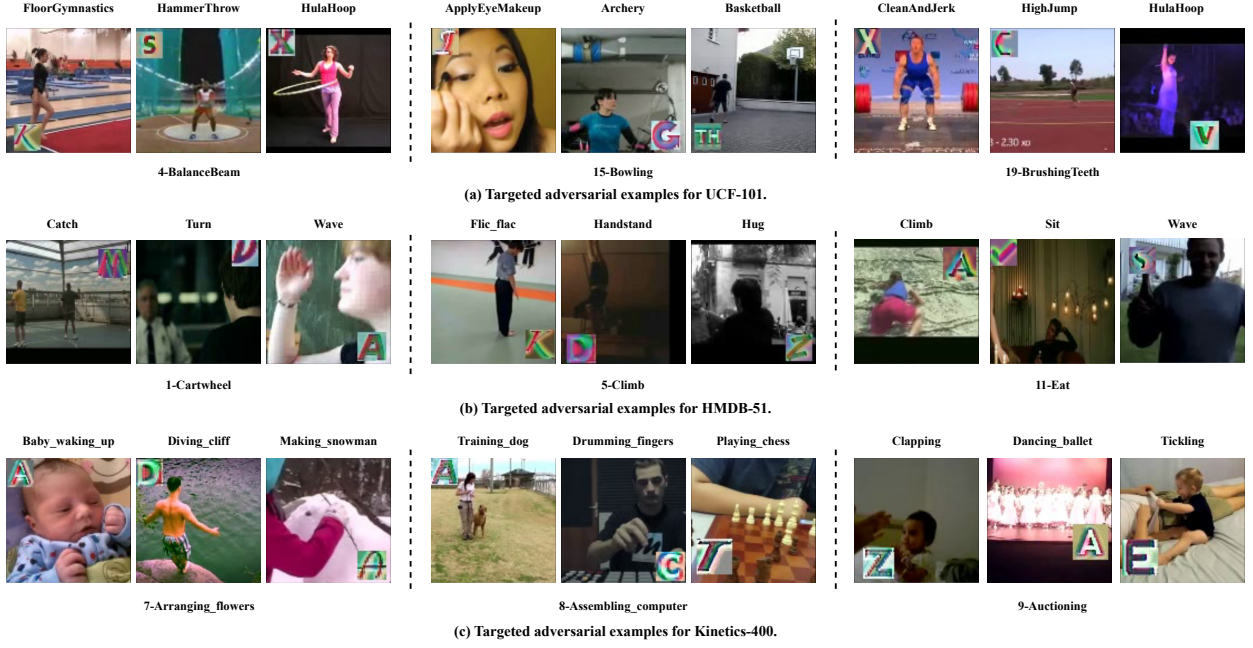


Fig. 4: Adversarial examples in targeted attacks on UCF-101, HMDB-51 and Kinetics-400.

TABLE 3: Results of SLA with various step size η_p .

η_p		UCF-101-Targeted					UCF-101-Untargeted				
		FR \uparrow	AQ $_1$	AQ $_2$	AQ $_3$	AQ $_4$	FR \uparrow	AQ $_1$	AQ $_2$	AQ $_3$	AQ $_4$
0.05	20%				10,528.7	13,112.6	100%		6,120.8	6,742.9	
0.1	35%				10,846.6	14,427.7	100%		4,866.8	5,747.4	
0.2	50%				4,632.7	8,393.9	100%		601.9	1,264.8	
0.3	40%	2,049.8 \pm 199.3	1,686.3 \pm 93.8		6,252.3	9,689.4	100%	1.2 \pm 0.2	683.5 \pm 89.8	1,207.3	1,823.2
0.4	40%				9,297.9	13,432.8	100%		1,064.6	3,676.8	
0.5	40%				12,528.2	16,446.2	100%		1,516.3	2,179.7	

5.3 Attack Performance

5.3.1 Qualitative Analysis

Figure 3 displays the adversarial samples generated by different methods. The PatchAttack [10] and Sparse-RS [14] are easily detected due to their lack of semantic nature in their patches. A significant drawback of Adv-watermark [11] is that it does not utilize RL to consider the interaction between the patch and video positions, which can affect the core semantics of the video. This is significantly different from the benign watermark positions that people add in their daily lives. BSC [13] is a good form of attack, but, like PatchAttack, it faces the challenge of limited search space, which seriously affects the performance of targeted attacks. Results in the subsequent Section 5.3.2 proves this. In addition, many video websites, such as YouTube and Bilibili, have bullet-screen shutdown functions, in which case the anomalies of BSC’s adversarial samples will be highlighted.

Figure 4 shows some adversarial examples of SLA in targeted attacks. The number before the hyphen represents the serial number of the target label. Most of the stylized logos added are located in the four corners of the video, which means that the main semantics of the original video are not affected. The natural semantics of the logo make it difficult for the patch to be detected when the current video is under attack - PatchAttack uses solid color patches for attacks, which can easily cause detection, and there is no unreal change in the global color - StyleFool [15] inevitably brings about unnatural color changes in the video. Figure 5 shows the adversarial examples of SLA in untargeted attacks. Different stylized logos can mislead target models into producing various classification results. Furthermore, the comparison of clean and adversarial video

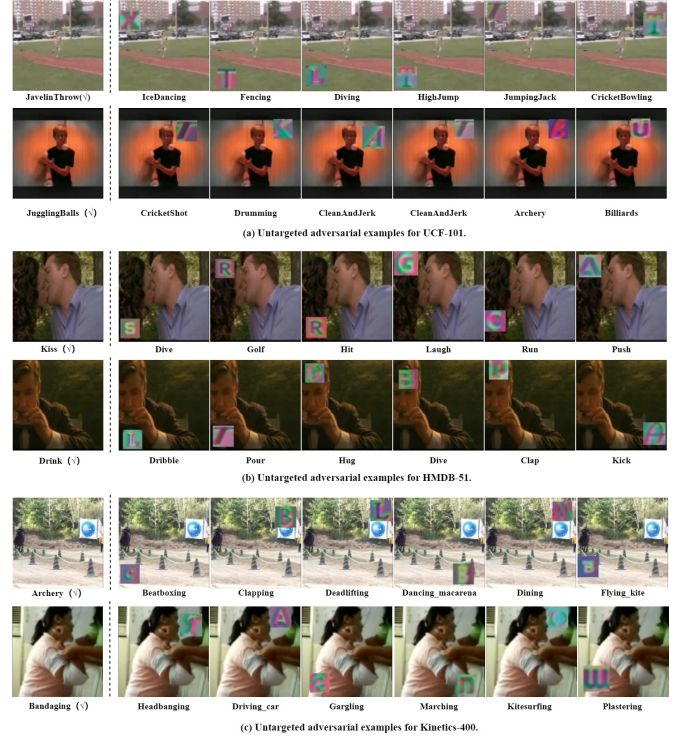


Fig. 5: Adversarial examples in untargeted attacks on UCF-101, HMDB-51 and Kinetics-400.

frames in targeted and untargeted scenarios are presented in Figure 6, Figure 7 and Figure 8.

5.3.2 Quantitative Analysis

Comparison of FR and Queries. Table 4, Table 5 and Table 6 report the numerical results of the attack performance of different methods in different datasets. In targeted attacks, in terms of FR performance, Adv-watermark exhibited the worst results (always below 5%), followed closely by PatchAttack. One possible reason



Fig. 6: Comparison of clean and adversarial video frames in targeted and untargeted attacks from UCF-101.

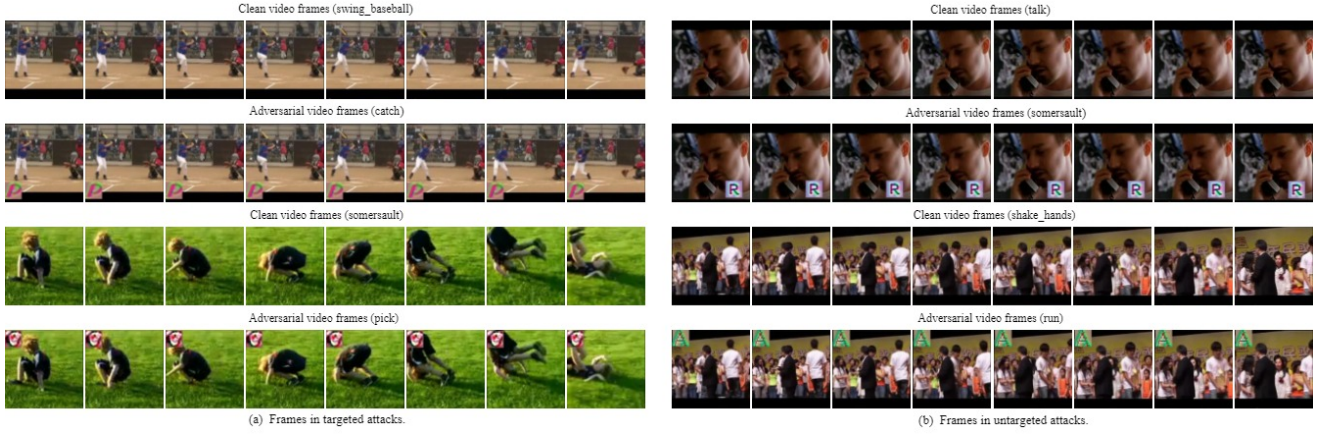


Fig. 7: Comparison of clean and adversarial video frames in targeted and untargeted attacks from HMDB-51.

for Adv-watermark’s poor performance is its excessive focus on stealthiness, such as the transparency of watermarks. BSC demonstrated relatively better performance compared to both Adv-watermark and PatchAttack across all three datasets, with especially notable results on HMDB-51 which includes the least classes. Consistent with the prior hypothesis, Kinetics-400, which boasts the largest number of classes, offers a more finely grained set of labels compared to UCF-101 and HMDB-51. This increased granularity presents a greater challenge for targeted attacks. Other methods, including Sparse-RS, LogoStyleFool, and **SLA**, also show this consistency in FR performance. Compared with **SLA**, Sparse-RS demonstrates the strongest competitiveness in FR. Sparse-RS exhibits a commonality with **SLA** in employing a derivative-free optimization approach (random search). However, the patches introduced by Sparse-RS lack semantic meaning and can be easily detected when human being is involved. More importantly, Sparse-RS does not employ covert handling of patches, such as the stylization offered by **SLA**. This deficiency results in more high-frequency variations in adversarial videos, which can make it challenging to evade defense mechanisms akin to LGS, as confirmed in Section 5.5.

As for the query consumption, PatchAttack and BSC require the most queries. Both methods require more than 20,000 queries in all datasets; the former requires over 30,000 queries on UCF-101, and the latter approaches 30,000 on Kinetics-400. Adv-watermark utilizes the fewest number of queries but suffers from a low FR. In

most cases, Sparse-RS does not require fewer queries compared to our method. Nonetheless, when compared to LogoStyleFool, **SLA** still manages to achieve significant improvements in both the query performance and FR across all scenarios. The possible reasons are as follows. In SA, utilized in **SLA**, the pixel region for each round of modification is larger than that in SimBA, which is adopted by LogostyleFool. Furthermore, SA can quickly find excellent candidate perturbations through random search. Most importantly, **SLA** can initialize better style images and stylized logos in the first two stages to reduce AQ and more effective by leveraging perturbation optimization after RL compared with Sparse-RS, Adv-watermark, PatchAttack and BSC.

In untargeted attacks, the most query-consuming method is PatchAttack, and its FR falls within the range of 80% to 90%. Adv-watermark exhibits poor performance in FR. Although Adv-watermark’s AQ number approaches the query requirement of 2AQ for the first two stages of **SLA**, almost all being less than 1,000, its FR is consistently at least 10% lower than that of **SLA** in all scenarios. **SLA** can achieve a FR exceeding 80% within just the first two stages, making it a viable variant for scenarios with more limited query budgets. Sparse-RS demonstrates only a slight advantage over **SLA** in terms of attack performance when attacking C3D on UCF-101. Sparse-RS shows instability on a more challenging dataset, Kinetics-400, where its FR is more than 20% lower compared to **SLA**. For BSC, its performance in terms of FR and the query efficiency is average. Furthermore, **SLA** demonstrates

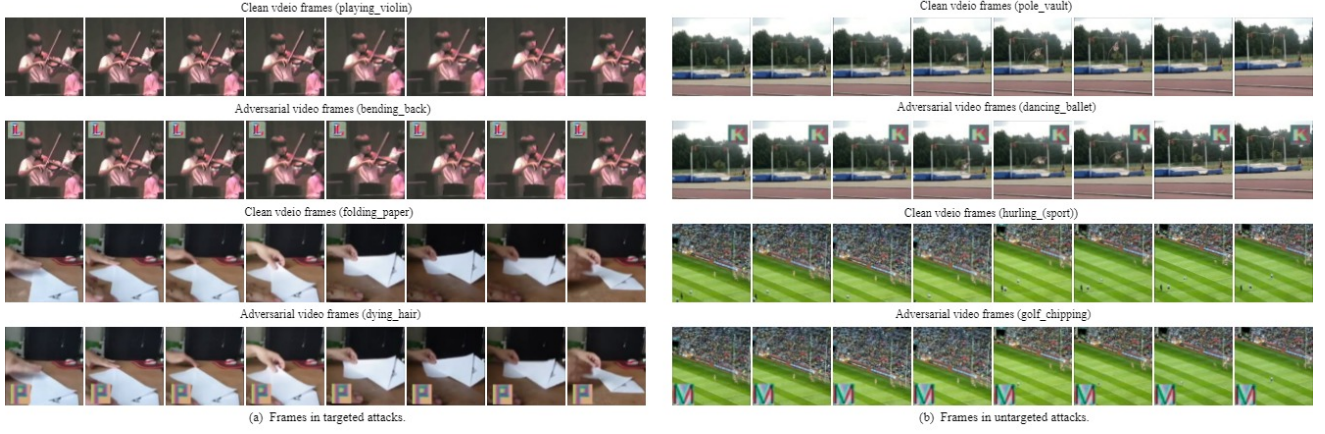


Fig. 8: Comparison of clean and adversarial video frames in targeted and untargeted attacks from Kinetics-400.

TABLE 4: Attack performance comparison on UCF-101. Metric details are provided in the experimental setup.

Model	Attack	UCF-101-Targeted				UCF-101-Untargeted			
		FR(² FR)↑	AQ(² AQ)↓	AOA↓	TI↓	FR(² FR)↑	AQ(² AQ)↓	AOA↓	TI↓
C3D	Sparse-RS	57%	14,013.2	4.98%	4.98	98%	213.8	4.98%	6.11
	Adv-watermark	2%	1,259.2	6.06%	4.66	69%	670.6	5.37%	3.73
	PatchAttack	5%	33,020.7	5.11%	75.62	80%	7,844.8	6.94%	102.06
	BSC	8%	27,608.4	7.15%	3.80	94%	2,228.1	7.26%	3.89
	LogoStyleFool	44%(8%)	22,993.9(4,124.4)	5.51%	3.76	94%(79%)	4,661.5(978.4)	6.52%	3.67
	SLA	65%(11%)	9,288.2(3,446.7)	4.88%	4.38	96%(80%)	3,313.6(782.7)	5.24%	3.66
I3D	Sparse-RS	53%	13,961.3	4.98%	5.10	88%	933.8	4.98%	6.88
	Adv-watermark	4%	1,417.5	4.56%	4.59	56%	932.7	4.67%	3.46
	PatchAttack	7%	32,604.8	4.67%	51.49	89%	4,082.1	5.97%	11.93
	BSC	9%	27,672.2	7.02%	3.68	81%	2,087.5	6.18%	3.87
	LogoStyleFool	37%(6%)	20,315.5(2,999.2)	5.47%	3.92	95%(83%)	3,955.3(889.7)	5.45%	4.01
	SLA	55%(8%)	10,443.7(2,732.1)	5.34%	4.28	97%(88%)	3,089.6(794.1)	5.39%	3.97

TABLE 5: Attack performance comparison on HMDB-51. Metric details are provided in the experimental setup.

Model	Attack	HMDB-51-Targeted				HMDB-51-Untargeted			
		FR(² FR)↑	AQ(² AQ)↓	AOA↓	TI↓	FR(² FR)↑	AQ(² AQ)↓	AOA↓	TI↓
C3D	Sparse-RS	71%	11,044.9	4.98%	4.78	97%	764.1	4.98%	5.31
	Adv-watermark	3%	1,038.1	4.24%	5.14	73%	610.2	4.35%	2.69
	PatchAttack	4%	28,829.1	5.17%	42.03	88%	1,934.3	6.01%	66.33
	BSC	25%	22,684.7	6.12%	4.95	97%	1,739.4	7.85%	3.50
	LogoStyleFool	46%(12%)	18,200.9(3,161.9)	5.14%	3.15	96%(86%)	3,396.6(901.6)	5.80%	3.03
	SLA	76%(14%)	7,124.1(2,854.6)	5.01%	3.67	98%(88%)	1,624.3(693.7)	5.59%	3.14
I3D	Sparse-RS	74%	8,217.0	4.98%	5.44	92%	2,010.5	4.98%	5.56
	Adv-watermark	4%	1,539.3	5.44%	4.01	78%	515.2	5.16%	3.65
	PatchAttack	12%	26,431.6	4.72%	303.34	89%	3,436.4	5.42%	15.79
	BSC	13%	26,311.3	6.19%	4.85	90%	3,137.5	6.89%	4.57
	LogoStyleFool	43%(11%)	20,612.8(4,723.9)	5.85%	3.52	94%(88%)	849.5(774.6)	5.48%	3.43
	SLA	66%(13%)	11,509.6(3,368.1)	6.08%	3.46	100%(96%)	624.9(614.9)	5.17%	3.40

its superiority over LogoStyleFool in FR in all scenarios. This is due to the high efficiency of SA’s random search.

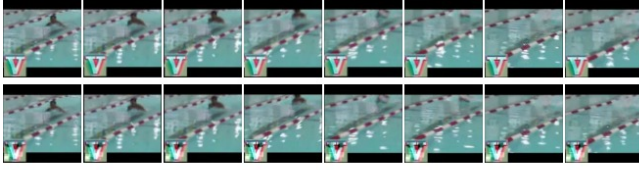
Comparison of AOA and TI. Table 4, Table 5 and Table 6 also provide the numerical results of *AOA* and *TI*. Attributed to the property of bullet-screen comments, the *AOA* associated BSC is maximal in all scenarios, typically exceeding 6% or 7%. The *AOA* of Sparse-RS is fixed since the size of patch is pre-specified. Specifically, for videos sized 112×112 , the patch size is set to 25×25 , while for videos sized 224×224 , the patch size is 50×50 . Adv-watermark exhibits the minimal *AOA* in most cases, benefiting from its transparency. Compared with PatchAttack and BSC, **SLA** typically demonstrates smaller *AOA*.

It is easy to notice the deficiency of PatchAttack in terms

of temporal consistency. One possible reason is the addition of solid color. Sparse-RS exhibits the same deficiency especially in high-resolution video dataset like kinetiks-400, which also can be attributed to the incorporation of patches that affect video consistency due to high-frequency variations. In contrast, Adv-watermark and BSC demonstrate better ability to maintain temporal consistency, as they design patches with transparency and semantics in mind. Another novel category of methods, LogoStyleFool and **SLA**, which superimposed stylized patches on clean videos, also show great temporal consistency, and in the vast majority of cases, these methods have the smallest *TI* values, indicating that the generated adversarial videos own the best fluency.

TABLE 6: Attack performance comparison on Kinetics-400. Metric details are provided in the experimental setup.

Model	Attack	Kinetics-400-Targeted				Kinetics-400-Untargeted			
		FR(² FR)↑	AQ(² AQ)↓	AOA↓	TI↓	FR(² FR)↑	AQ(² AQ)↓	AOA↓	TI↓
C3D	Sparse-RS	59%	14,971.2	4.98%	7.75	64%	197.5	4.98%	11.56
	Adv-watermark	2%	2,062.1	6.41%	5.94	75%	604.4	4.90%	5.02
	PatchAttack	3%	25,121.1	4.64%	25.57	86%	4,334.4	6.78%	19.71
	BSC	3%	29,124.8	6.58%	5.08	84%	2,217.6	6.70%	5.61
	LogoStyleFool	22%(4%)	21,093.3(7,559.1)	4.91%	5.39	91%(82%)	1,824.9(930.1)	5.91%	5.44
	SLA	39%(5%)	17,641.3(5,601.4)	4.42%	5.01	97%(87%)	1,552.4(900.8)	6.18%	4.33
I3D	Sparse-RS	31%	22,723.9	4.98%	6.93	79%	4,531.0	4.98%	9.63
	Adv-watermark	3%	1,866.9	4.79%	5.29	66%	780.5	4.45%	5.54
	PatchAttack	5%	21,585.4	4.77%	12.47	81%	5,839.9	7.31%	141.81
	BSC	6%	29,409.4	7.12%	5.58	76%	2,874.0	7.70%	5.65
	LogoStyleFool	20%(6%)	23,602.7(6,221.6)	4.62%	5.44	83%(82%)	4,422.4(1,471.4)	5.76%	5.69
	SLA	33%(7%)	10,921.8(5,283.5)	3.77%	5.21	95%(83%)	3,679.9(1,224.3)	5.82%	5.49



(a) Comparison of adversarial examples from UCF-101 in perturbation optimization scenarios.



(b) Comparison of adversarial examples from HMDB-51 in perturbation optimization scenarios.



(c) Comparison of adversarial examples from Kinetics-400 in perturbation optimization scenarios.

Fig. 9: Comparison of adversarial video frames when perturbation optimization is needed.

5.4 Attack Visualization

To display the impact of **SLA** on the classifier, Grad-CAM [69] is used to visualize the regions of interest in the target model when attacking C3D on UCF-101. Figure 10 shows the visualization results. In each small figure, the left image represents a frame from a clean (adversarial) video, while the right image shows the region of interest that the model focuses on for that particular frame of the clean (adversarial) video. The prediction results of the classifier is labeled above each small figure. Visually, it is apparent that the adversarial examples created by **SLA** exhibits significant power to distort the model’s judgments. Specifically, the attacked model’s focus may not solely be confined to the stylized logo region; it could also be inadvertently drawn to extraneous areas, since once an adversarial video capable of misleading the model is obtained, its confidence score of the target class will no longer be increased.

5.5 Countermeasure

In this subsection, two SOTA defense methods that are designed for patch-based attacks are selected to evaluate **SLA**’s ability to counter these defenses. LGS [57] regularizes gradients in the estimated perturbation region before feeding the video to the model for inference. The objective of PC [58] is to identify a pair of benign

TABLE 7: Fooling rate (↑) of defense performance. The fooling rate is averaged on both targeted and untargeted attacks.

Model	Attack	UCF-101		HMDB-51		Kinetics-400	
		LGS	PC	LGS	PC	LGS	PC
C3D	Sparse-RS	33.0%	48.5%	28.0%	34.0%	31.0%	39.5%
	Adv-watermark	34.0%	41.0%	32.0%	37.0%	41.0%	36.5%
	PatchAttack	27.0%	39.0%	49.5%	41.5%	56.0%	44.0%
	BSC	30.0%	42.5%	52.0%	41.5%	44.5%	42.0%
	SLA	52.5%	55.5%	56.0%	45.0%	52.5%	46.5%
I3D	Sparse-RS	32.0%	36.5%	26.0%	39.5%	22.0%	50.5%
	Adv-watermark	36.0%	34.0%	37.0%	58.0%	32.0%	39.0%
	PatchAttack	36.5%	35.0%	47.5%	48.5%	43.0%	40.0%
	BSC	40.5%	47.5%	49.0%	55.5%	44.0%	42.5%
	SLA	42.5%	42.0%	52.5%	59.5%	45.0%	41.0%

patches that conceal adversarial videos in a two-round masking manner. LGS and PC are extended to video. FR is employed to assess the robustness of different methods against adversarial defenses.

Table 7 reports the numerical performance of different attack methods against defenses. **SLA** includes a perturbation optimization stage that introduces square-shaped perturbations to the logo area, potentially rendering the content of the logo irregular. Figure 9 shows the comparison results when perturbation optimization is needed. Attacks such as Adv-watermark [11], BSC [13], and

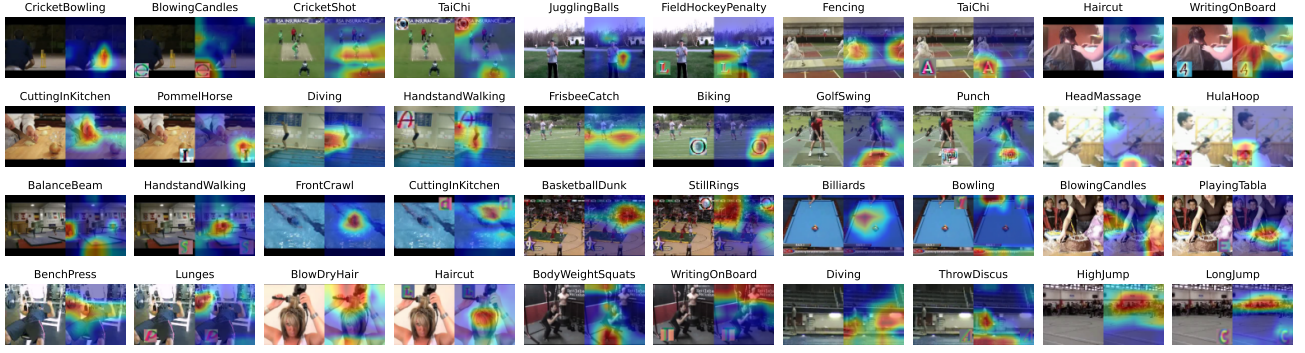


Fig. 10: Grad-CAM visualizations of **SLA**. Top two rows: targeted attacks, bottom two rows: untargeted attacks.

TABLE 8: Ablation results of **SLA**.

Attack scenario	UCF-101-Targeted					UCF-101-Untargeted				
	FR(² FR)↑	AQ ₁	AQ ₂	AQ ₃	AQ(² AQ)↓	FR(² FR)↑	AQ ₁	AQ ₂	AQ ₃	AQ(² AQ)↓
Random style image	31%(6%)	0	2,185.4	13,786.8	15,972.2(2,185.4)	92%(74%)	0	682.3	2,055.7	2,738.0(682.3)
Solid color initialization	36%(6%)	2,109.9	2,056.6	9,802.1	13,968.6(4,166.5)	87%(72%)	1.1	1,062.6	4,587.9	5,651.6(1,063.7)
Vertical strips initialization	49%(9%)	2,317.0	2,074.6	9,019.2	13,410.8(4,391.6)	94%(86%)	1.1	784.1	2,218.2	3,003.4(785.2)
$\mu_a = 0$	58%(9%)	2,079.4	1,839.0	8,017.5	11,935.9(3,918.4)	90%(82%)	1.0	916.3	3,305.4	4,222.7(917.3)
$\mu_d = 0$	62%(11%)	2,061.6	1,715.7	7,030.7	10,808.0(3,777.3)	90%(80%)	1.0	800.1	3,315.1	4,116.2(801.1)
Random step direction	57%(7%)	1,821.7	2,022.3	9,025.9	12,869.9(3,844.0)	91%(82%)	1.2	1,020.9	3,299.8	4,321.9(1,022.1)

PatchAttack [10] provide a smoother perturbation because they do not include the perturbation optimization, which, however, results in poor performance in targeted attacks. Furthermore, **SLA** still exhibits a certain degree of superiority in resisting defenses in most cases, even though some samples' logos have been subjected to irregular perturbations. Therefore, the performance of **SLA** can be regarded as a positive result. In addition, constructing a perturbation optimization for BSC and PatchAttack could potentially trigger human detection alarms (due to the more conspicuous nature of the bullet-screen comments) and highlight the presence of purely patches. Current patch-based defense methods still have a certain distance to go before they can be practically applied.

5.6 Ablation Study

To validate the effectiveness of different components in **SLA**, experiments are conducted on the UCF-101 [33] dataset, considering 6 different variations (abbreviated as $A \sim F$) in three stages. The descriptions of these variations are as follows.

A: Random style image (Stage 1): Random style images are used, thus skipping the use of perturbations in the first stage. *B: Solid color initialization (Stage 1):* Solid colors are adopted instead of random initialization. *C: Vertical strips initialization (Stage 1):* Vertical strip with a width of 1 is utilized, and the color of each strip (p) is sampled uniformly from $\{-\eta, +\eta\}^c$, where c denotes the number of color channels in the style image. *D: $u_a = 0$ (Stage 2):* The constraint on the size of the logo is removed. *E: $u_d = 0$ (Stage 2):* The constraint on the distance of the logo from the four corners of the video is removed. *F: Random step direction (Stage 3):* Compared to the initial pixels, in each round, any pixel can change by any one of $\{-\eta_p, 0, \eta_p\}$.

Impact of the Style Reference Selection (Stage 1). As evidenced by Table 8, variant A can be considered as skipping Stage 1, although variant A saves the required queries for selecting style images, the lack of ability to carry target class information leads to sharp decrease in targeted attack efficiency. Especially

during the perturbation optimization stage, the number of queries exceeded 13,000. On the other hand, thanks to the ability of the roughly randomized style images to mislead the classifier, the efficiency of untargeted attacks has been improved. Therefore, A can serve as an improved variant of **SLA** in untargeted attacks. Variants B and C mainly focus on exploring different initialization strategies for style images. Like A, they both perform poorly in targeted attacks. Specifically, the monotonous color from B makes perturbation optimization more difficult, resulting in more than 9,000(4,500) queries in Stage 3 for targeted (untargeted) attacks. For variant C, although some studies [32], [54] in the field of image processing indicate that CNNs have shown a particular sensitivity to strip-based perturbations, the vertical strips are ineffective. One possible reason is the increased dimensionality from images to videos.

Impact of the RL-based Logo Style Transfer (Stage 2).

In theory, variants D and E directly affect the core semantics of video, reducing the naturalness of the video, and may trigger people's awareness due to the size or position of the superimposed logo being not restricted. Define that the average logo area $\bar{a} = \sum_i k_i^2 hw$ and the average minimum distance to the corners $\bar{d}_m = \sum_i d_{m,i}$, where i represents the i -th adversarial video. The sums are taken over all adversarial videos. Experimental results in Table 8 show that these averages increase significantly. Specifically, compared with \bar{a} of 853.0(657.3) and \bar{d}_m of 8.8(14.8) for targeted (untargeted) attacks in **SLA**, \bar{a} becomes 917.1(731.3) for targeted (untargeted) attacks in variants D, and \bar{d}_m becomes 35.4(23.2) for targeted (untargeted) attacks in variants E. Since both of the two variants can make the logo too conspicuous and may affect the semantics of the videos, these two variants are not adopted.

Impact of the Perturbation Optimization (Stage 3). Variant F can result in disordered perturbation optimization, which may cause a sharp increase in the required queries during Stage 3. The numerical results from Table 8 confirm this conjecture. Specifically, when comparing the AQ_3 (5,841.5) in **SLA** to variant F, the AQ_3

(9,025.9) in variant F is 54.5% higher than that in **SLA** for targeted attacks. In untargeted attacks the AQ_3 (3,299.8) in variant F has increased by more than 30.0% compared to the AQ_3 (2,530.9) in **SLA**.

5.7 User Study

To verify the naturalness of the adversarial videos generated by **SLA** and to determine whether they affect human understanding of video content. Two sets of user studies are conducted to evaluate the naturalness and semanticity of adversarial samples.

5.7.1 Preparation

30 videos (10 each from each dataset) in Section 5 are respectively selected for naturalness test and semanticity test. These videos are denoted as the naturalness set and semanticity set, respectively. Both sets consist of 15 clean videos and 15 adversarial videos. Since the naturalness test is used to evaluate whether the attack by **SLA** can cause human detection, the videos are played one by one. However, the purpose of the semanticity test is to show whether the patches added to the video affect the semantics of the video, the clean video and the corresponding adversarial video are simultaneously played as paired videos.

Platform and Subjects. Amazon Mechanical Turk (AMT) was chosen as the platform for the online survey. It is a crowdsourcing platform under Amazon. When a user posts a request, AMT sends this request to task performers. The performers then respond, and the server relays the responses back to the requester. This survey recruited 100 anonymous participants, all of whom are over 18 years old, with English as their native language, and they have maintained at least a 95% approval rate for their past responses. They were evenly divided into two groups to score naturalness and semanticity to avoid bias.

5.7.2 Questionnaire Design

The surveys are all answered by selecting options, with five options provided for each question, and participants can only choose one answer per question. In the naturalness test, after watching the video, participants are required to evaluate the video based on a Likert scale [70] from 1 to 5, representing “very unnatural”, “somehow unnatural”, “neutral”, “somewhat natural”, and “very natural”, respectively. Note that in the naturalness test, the survey does not inform participants in advance about which video is attacked by **SLA**. In the semanticity test, videos are presented in pairs from the same video, and the survey informs the participants which video is attacked, with the focus of the participants’ scoring based solely on whether the semantics of the video after the attack is impacted. Similarly, they are required to rate the video from 1 to 5, representing “very impactful”, “somewhat impactful”, “neutral”, “somewhat unimpactful”, and “very unimpactful”, respectively. Additionally, for compensation, the participants are paid by \$0.8 per question for the naturalness test and \$1.2 per question for the semanticity test. The slightly higher payment for the latter is to compensate for the participants in that group who need to watch two videos to answer a question.

5.7.3 Results Analyses

Figure 11 displays the evaluation results for UCF-101, HMDB-51, and Kinetics-400, respectively. In each subplot, the x-axis represents the score value, and the y-axis represents the proportion of videos that are rated above a given score relative to the total

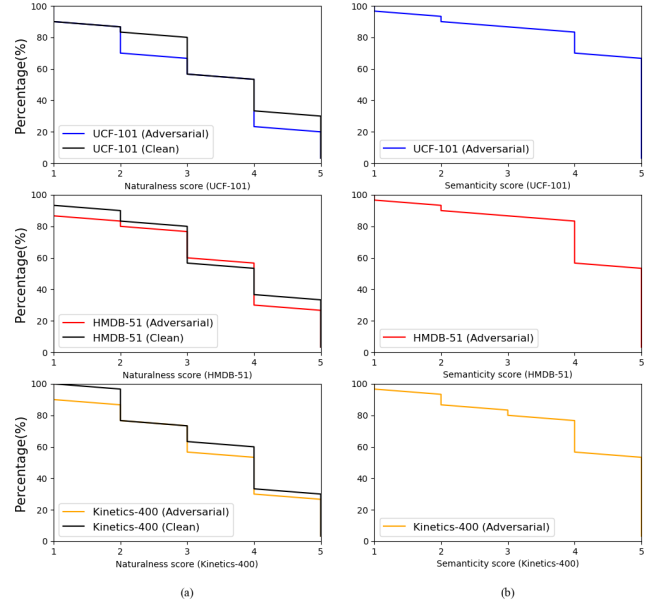


Fig. 11: Statistical distributions of naturalness and semanticity scores.

number of selected videos. Specifically, given a vertical line at $x = score$, where $score \in \{1, 2, 3, 4, 5\}$, the highest y-value that intersects the curve is taken as the intersection point. Therefore, the more the curve in the plot is distributed towards the upper right, the better the overall evaluation of the videos by the participants.

Naturalness. Figure 11(a) shows the participants’ naturalness scores for adversarial and clean videos. It can be intuitively observed that among the three datasets, the score distributions for adversarial and clean videos are quite close, with clean videos having a slight advantage in naturalness. In HMDB-51, the percentage of adversarial videos at score 4 is even higher than that of clean videos. These results implies that videos attacked by **SLA** still appear natural and are difficult for humans to detect. This is largely attributed to **SLA**’s stylization strategy, which ensures that the added logos do not stand out conspicuously and clash with the clean videos.

Semanticity. Figure 11(b) shows the results of the semantic impact of adversarial videos generated by **SLA** on the videos. Among the three datasets, more than 50% of the adversarial videos were considered “very unimpactful” by participants. This figure is even over 60% on UCF-101. This means that the semantics of more than half of the videos are not affected by **SLA**. Over 80% (including “very unimpactful”) of the videos in UCF-101 and HMDB-51, and over 70% (including “very unimpactful”) in Kinetics-400 were considered “somewhat unimpactful”. This implies that in UCF-101 and HMDB-51, less than 20% of the adversarial videos have a more neutral or significant semantic impact (less than 30% in Kinetics-400), demonstrating that under the guidance of RL, **SLA** makes very cautious selections regarding the size and position of the logos, which limits the perturbation area to be as small as possible, and to the corners of the video. The semanticity test proves that the design of the reward function is reasonable.

The two sets of user studies conducted demonstrate the powerful capabilities of **SLA**-generated adversarial videos in terms of naturalness and semantics preservation. This novel stylized-patch attack, while maintaining strong attacking power, also takes into account stealthiness very well, offering strong practicality for

adversaries. The users' responses are sufficient to show that this type of attack deserves attention from the security community.

6 CONCLUSION

This paper presents a query-efficient video adversarial attack against video recognition models. In contrast to prior works that relies solely on style-transfer-based or patch-based adversarial attacks, our study introduce a novel approach by integrating a stylized logo into the video's corner, acting as an adversarial patch. This method, dubbed as **SLA**, has three key aspects. First, a refined random-search-based strategy that combines SimBA with Square Attack to select style reference. Next, a RL-driven style transfer is deployed to search the optimal attributes of the patch. Last, a perturbation optimizer named Logo-SSA optimizes the adversarial video in a step-by-step manner. Extensive experiments verify the superior outperformance of **SLA** on both attack efficiency to the state-of-the-art methods and robustness against two existing defenses against patch attacks. **SLA**, as a novel method that combines style-transfer-based and patch-based approaches, can provide insights for the study of stylized-patch-attacks in the security community. Future work will focus on exploring potential defenses towards such stylized-patch attack.

ACKNOWLEDGMENT

The authors thank anonymous reviewers for their feedback that helped improve the paper. This work was supported in part by CSIRO's Data61.

REFERENCES

- [1] S. Ji, W. Xu, M. Yang, and K. Yu, "3d convolutional neural networks for human action recognition," *IEEE Transactions on Pattern Analysis and Machine Intelligence*, vol. 35, no. 1, pp. 221–231, 2012.
- [2] Z.-Q. Zhao, P. Zheng, S.-t. Xu, and X. Wu, "Object detection with deep learning: A review," *IEEE Transactions on Neural Networks and Learning Systems*, vol. 30, no. 11, pp. 3212–3232, 2019.
- [3] D. Nilsson and C. Sminchisescu, "Semantic video segmentation by gated recurrent flow propagation," in *Proceedings of the IEEE Conference on Computer Vision and Pattern Recognition*, 2018, pp. 6819–6828.
- [4] S. Kuutti, R. Bowden, Y. Jin, P. Barber, and S. Fallah, "A survey of deep learning applications to autonomous vehicle control," *IEEE Transactions on Intelligent Transportation Systems*, vol. 22, no. 2, pp. 712–733, 2020.
- [5] M. Prunella, R. M. Scardigno, D. Buongiorno, A. Brunetti, N. Longo, R. Carli, M. Dotoli, and V. Bevilacqua, "Deep learning for automatic vision-based recognition of industrial surface defects: a survey," *IEEE Access*, vol. 11, pp. 43 370–43 423, 2023.
- [6] S. K. Zhou, H. Greenspan, C. Davatzikos, J. S. Duncan, B. Van Ginneken, A. Madabhushi, J. L. Prince, D. Rueckert, and R. M. Summers, "A review of deep learning in medical imaging: Imaging traits, technology trends, case studies with progress highlights, and future promises," *Proceedings of the IEEE*, vol. 109, no. 5, pp. 820–838, 2021.
- [7] I. J. Goodfellow, J. Shlens, and C. Szegedy, "Explaining and harnessing adversarial examples," *arXiv preprint arXiv:1412.6572*, 2014.
- [8] X. Wei, J. Zhu, S. Yuan, and H. Su, "Sparse adversarial perturbations for videos," in *Proceedings of the AAAI Conference on Artificial Intelligence*, vol. 33, no. 01, 2019, pp. 8973–8980.
- [9] C. Szegedy, W. Zaremba, I. Sutskever, J. Bruna, D. Erhan, I. Goodfellow, and R. Fergus, "Intriguing properties of neural networks," in *Proceedings of the International Conference on Learning Representations*, 2014.
- [10] C. Yang, A. Kortylewski, C. Xie, Y. Cao, and A. Yuille, "Patchattack: A black-box texture-based attack with reinforcement learning," in *Proceedings of the European Conference on Computer Vision*. Springer, 2020, pp. 681–698.
- [11] X. Jia, X. Wei, X. Cao, and X. Han, "Adv-watermark: A novel watermark perturbation for adversarial examples," in *Proceedings of the 28th ACM International Conference on Multimedia*, 2020, pp. 1579–1587.
- [12] H. Yan and X. Wei, "Efficient sparse attacks on videos using reinforcement learning," in *Proceedings of the 29th ACM International Conference on Multimedia*, 2021, pp. 2326–2334.
- [13] K. Chen, Z. Wei, J. Chen, Z. Wu, and Y.-G. Jiang, "Attacking video recognition models with bullet-screen comments," in *Proceedings of the AAAI Conference on Artificial Intelligence*, vol. 36, no. 1, 2022, pp. 312–320.
- [14] F. Croce, M. Andriushchenko, N. D. Singh, N. Flammarion, and M. Hein, "Sparse-rs: a versatile framework for query-efficient sparse black-box adversarial attacks," in *Proceedings of the AAAI Conference on Artificial Intelligence*, vol. 36, no. 6, 2022, pp. 6437–6445.
- [15] Y. Cao, X. Xiao, R. Sun, D. Wang, M. Xue, and S. Wen, "Stylefool: Fooling video classification systems via style transfer," in *Proceedings of the IEEE Symposium on Security and Privacy*. IEEE, 2023, pp. 1631–1648.
- [16] X. Gong, Z. Fang, B. Li, T. Wang, Y. Chen, and Q. Wang, "Palette: Physically-realizable backdoor attacks against video recognition models," *IEEE Transactions on Dependable and Secure Computing*, 2023.
- [17] X. Gong, Z. Wang, Y. Chen, M. Xue, Q. Wang, and C. Shen, "Kaleidoscope: Physical backdoor attacks against deep neural networks with rgb filters," *IEEE Transactions on Dependable and Secure Computing*, vol. 20, no. 6, pp. 4993–5004, 2023.
- [18] R. Duan, X. Ma, Y. Wang, J. Bailey, A. K. Qin, and Y. Yang, "Adversarial camouflage: Hiding physical-world attacks with natural styles," in *Proceedings of the IEEE Conference on Computer Vision and Pattern Recognition*, 2020, pp. 1000–1008.
- [19] N. Inkawhich, M. Inkawhich, Y. Chen, and H. Li, "Adversarial attacks for optical flow-based action recognition classifiers," *arXiv preprint arXiv:1811.11875*, 2018.
- [20] S. Li, A. Neupane, S. Paul, C. Song, S. V. Krishnamurthy, A. K. Roy-Chowdhury, and A. Swami, "Stealthy adversarial perturbations against real-time video classification systems," in *Proceedings of the Symposium on Network and Distributed Systems Security*, 2019.
- [21] Z. Chen, L. Xie, S. Pang, Y. He, and Q. Tian, "Appending adversarial frames for universal video attack," in *Proceedings of the IEEE/CVF Winter Conference on Applications of Computer Vision*, 2021, pp. 3199–3208.
- [22] J.-W. Chang, M. Javaheripi, S. Hidano, and F. Koushanfar, "Rovisq: Reduction of video service quality via adversarial attacks on deep learning-based video compression," in *Proceedings of the Symposium on Network and Distributed Systems Security*, 2022.
- [23] W. Brendel, J. Rauber, and M. Bethge, "Decision-based adversarial attacks: Reliable attacks against black-box machine learning models," in *Proceedings of the International Conference on Learning Representations*, 2018.
- [24] M. Cheng, T. Le, P.-Y. Chen, J. Yi, H. Zhang, and C.-J. Hsieh, "Query-efficient hard-label black-box attack: An optimization-based approach," *arXiv preprint arXiv:1807.04457*, 2018.
- [25] J. Chen, M. I. Jordan, and M. J. Wainwright, "Hopskipjumpattack: A query-efficient decision-based attack," in *Proceedings of the IEEE Symposium on Security and Privacy*. IEEE, 2020, pp. 1277–1294.
- [26] W. Chen, Z. Zhang, X. Hu, and B. Wu, "Boosting decision-based black-box adversarial attacks with random sign flip," in *Proceedings of the European Conference on Computer Vision*. Springer, 2020, pp. 276–293.
- [27] J. Chen and Q. Gu, "Rays: A ray searching method for hard-label adversarial attack," in *Proceedings of the 26th ACM SIGKDD International Conference on Knowledge Discovery & Data Mining*, 2020, pp. 1739–1747.
- [28] A. Ilyas, L. Engstrom, A. Athalye, and J. Lin, "Black-box adversarial attacks with limited queries and information," in *Proceedings of the International Conference on Machine Learning*. PMLR, 2018, pp. 2137–2146.
- [29] S. Liu, P.-Y. Chen, X. Chen, and M. Hong, "signsgd via zeroth-order oracle," in *Proceedings of the International Conference on Learning Representations*, 2019.
- [30] A. Ilyas, L. Engstrom, and A. Madry, "Prior convictions: Black-box adversarial attacks with bandits and priors," *Proceedings of the International Conference on Learning Representations*, 2018.
- [31] C. Guo, J. Gardner, Y. You, A. G. Wilson, and K. Weinberger, "Simple black-box adversarial attacks," in *Proceedings of the International Conference on Machine Learning*. PMLR, 2019, pp. 2484–2493.
- [32] M. Andriushchenko, F. Croce, N. Flammarion, and M. Hein, "Square attack: a query-efficient black-box adversarial attack via random search," in *Proceedings of the European Conference on Computer Vision*. Springer, 2020, pp. 484–501.
- [33] K. Soomro, A. R. Zamir, and M. Shah, "Ucf101: A dataset of 101 human actions classes from videos in the wild," *arXiv preprint arXiv:1212.0402*, 2012.

- [34] H. Kuehne, H. Jhuang, E. Garrote, T. Poggio, and T. Serre, “Hmdb: a large video database for human motion recognition,” in *Proceedings of the IEEE International Conference on Computer Vision*. IEEE, 2011, pp. 2556–2563.
- [35] W. Kay, J. Carreira, K. Simonyan, B. Zhang, C. Hillier, S. Vijayarasmihnan, F. Viola, T. Green, T. Back, P. Natsev *et al.*, “The kinetics human action video dataset,” *arXiv preprint arXiv:1705.06950*, 2017.
- [36] Y. Cao, Z. Zhao, X. Xiao, D. Wang, M. Xue, and J. Lu, “Logostylefool: Vitiating video recognition systems via logo style transfer,” in *Proceedings of the AAAI Conference on Artificial Intelligence*, vol. 38, no. 2, 2024, pp. 945–953.
- [37] L. Jiang, X. Ma, S. Chen, J. Bailey, and Y.-G. Jiang, “Black-box adversarial attacks on video recognition models,” in *Proceedings of the 27th ACM International Conference on Multimedia*, 2019, pp. 864–872.
- [38] Z. Wei, J. Chen, X. Wei, L. Jiang, T.-S. Chua, F. Zhou, and Y.-G. Jiang, “Heuristic black-box adversarial attacks on video recognition models,” in *Proceedings of the AAAI Conference on Artificial Intelligence*, vol. 34, no. 07, 2020, pp. 12 338–12 345.
- [39] D. Kumar, C. Kumar, C. W. Seah, S. Xia, and M. Shao, “Finding achilles’ heel: Adversarial attack on multi-modal action recognition,” in *Proceedings of the 28th ACM International Conference on Multimedia*, 2020, pp. 3829–3837.
- [40] R. Pony, I. Naeh, and S. Mannor, “Over-the-air adversarial flickering attacks against video recognition networks,” in *Proceedings of the IEEE Conference on Computer Vision and Pattern Recognition*, 2021, pp. 515–524.
- [41] K. Jiang, Z. Chen, X. Zhou, J. Zhang, L. Hong, J. Wang, B. Li, Y. Wang, and W. Zhang, “Towards decision-based sparse attacks on video recognition,” in *Proceedings of the 31st ACM International Conference on Multimedia*, 2023, pp. 1443–1454.
- [42] Y. Xu, X. Liu, M. Yin, T. Hu, and K. Ding, “Sparse adversarial attack for video via gradient-based keyframe selection,” in *Proceedings of the IEEE International Conference on Acoustics, Speech and Signal Processing*. IEEE, 2022, pp. 2874–2878.
- [43] G. Wu, Y. Xu, J. Li, Z. Shi, and X. Liu, “Imperceptible adversarial attack with multigranular spatiotemporal attention for video action recognition,” *IEEE Internet of Things Journal*, vol. 10, no. 20, pp. 17 785–17 796, 2023.
- [44] Z. Wang, C. Sha, and S. Yang, “Reinforcement learning based sparse black-box adversarial attack on video recognition models,” in *Proceedings of International Joint Conference on Artificial Intelligence*, 2021.
- [45] X. Wei, H. Yan, and B. Li, “Sparse black-box video attack with reinforcement learning,” *International Journal of Computer Vision*, vol. 130, no. 6, pp. 1459–1473, 2022.
- [46] X. Wei, S. Wang, and H. Yan, “Efficient robustness assessment via adversarial spatial-temporal focus on videos,” *IEEE Transactions on Pattern Analysis and Machine Intelligence*, vol. 45, no. 9, pp. 10 898–10 912, 2023.
- [47] J. Chen, T. Chen, X. Xu, J. Zhang, Y. Yang, and H. T. Shen, “Coreset learning based sparse black-box adversarial attack for video recognition,” *IEEE Transactions on Information Forensics and Security*, 2023.
- [48] A. Hertzmann, C. E. Jacobs, N. Oliver, B. Curless, and D. H. Salesin, “Image analogies,” in *Seminal Graphics Papers: Pushing the Boundaries, Volume 2*, 2023, pp. 557–570.
- [49] L. A. Gatys, A. S. Ecker, and M. Bethge, “A neural algorithm of artistic style,” *arXiv preprint arXiv:1508.06576*, 2015.
- [50] M. Ruder, A. Dosovitskiy, and T. Brox, “Artistic style transfer for videos and spherical images,” *International Journal of Computer Vision*, vol. 126, no. 11, pp. 1199–1219, 2018.
- [51] J. Johnson, A. Alahi, and L. Fei-Fei, “Perceptual losses for real-time style transfer and super-resolution,” in *Proceedings of the European Conference on Computer Vision*. Springer, 2016, pp. 694–711.
- [52] H. Huang, H. Wang, W. Luo, L. Ma, W. Jiang, X. Zhu, Z. Li, and W. Liu, “Real-time neural style transfer for videos,” in *Proceedings of the IEEE Conference on Computer Vision and Pattern Recognition*, 2017, pp. 783–791.
- [53] A. Fawzi and P. Frossard, “Measuring the effect of nuisance variables on classifiers,” in *Proceedings of the British Machine Vision Conference*, 2016, pp. 137–1.
- [54] D. Yin, R. Gontijo Lopes, J. Shlens, E. D. Cubuk, and J. Gilmer, “A fourier perspective on model robustness in computer vision,” in *Proceedings of the Advances in Neural Information Processing Systems*, 2019.
- [55] O. Russakovsky, J. Deng, H. Su, J. Krause, S. Satheesh, S. Ma, Z. Huang, A. Karpathy, A. Khosla, M. Bernstein *et al.*, “Imagenet large scale visual recognition challenge,” *International Journal of Computer Vision*, vol. 115, pp. 211–252, 2015.
- [56] K. Jiang, Z. Chen, H. Huang, J. Wang, D. Yang, B. Li, Y. Wang, and W. Zhang, “Efficient decision-based black-box patch attacks on video recognition,” in *Proceedings of the IEEE International Conference on Computer Vision*, 2023, pp. 4379–4389.
- [57] M. Naseer, S. Khan, and F. Porikli, “Local gradients smoothing: Defense against localized adversarial attacks,” in *Proceedings of the IEEE/CVF Winter Conference on Applications of Computer Vision*. IEEE, 2019, pp. 1300–1307.
- [58] C. Xiang, S. Mahloujifar, and P. Mittal, “{PatchCleanser}: Certifiably robust defense against adversarial patches for any image classifier,” in *31st USENIX Security Symposium (USENIX Security 22)*, 2022, pp. 2065–2082.
- [59] K. Xu, Y. Xiao, Z. Zheng, K. Cai, and R. Nevatia, “Patchzero: Defending against adversarial patch attacks by detecting and zeroing the patch,” in *Proceedings of the IEEE/CVF Winter Conference on Applications of Computer Vision*, 2023, pp. 4632–4641.
- [60] L. Wang, Y. Xiong, Z. Wang, Y. Qiao, D. Lin, X. Tang, and L. Van Gool, “Temporal segment networks for action recognition in videos,” *IEEE Transactions on Pattern Analysis and Machine Intelligence*, vol. 41, no. 11, pp. 2740–2755, 2018.
- [61] D. Tran, L. Bourdev, R. Fergus, L. Torresani, and M. Paluri, “Learning spatiotemporal features with 3d convolutional networks,” in *Proceedings of the IEEE International Conference on Computer Vision*, 2015, pp. 4489–4497.
- [62] X. Wang, R. Girshick, A. Gupta, and K. He, “Non-local neural networks,” in *Proceedings of the IEEE Conference on Computer Vision and Pattern Recognition*, 2018, pp. 7794–7803.
- [63] C. Yang, Y. Xu, J. Shi, B. Dai, and B. Zhou, “Temporal pyramid network for action recognition,” in *Proceedings of the IEEE Conference on Computer Vision and Pattern Recognition*, 2020, pp. 591–600.
- [64] J. Carreira and A. Zisserman, “Quo vadis, action recognition? a new model and the kinetics dataset,” in *Proceedings of the IEEE Conference on Computer Vision and Pattern Recognition*, 2017, pp. 6299–6308.
- [65] A. Sage, E. Agustsson, R. Timofte, and L. Van Gool, “Logo synthesis and manipulation with clustered generative adversarial networks,” in *Proceedings of the IEEE Conference on Computer Vision and Pattern Recognition*, 2018, pp. 5879–5888.
- [66] K. Simonyan, “Very deep convolutional networks for large-scale image recognition,” *arXiv preprint arXiv:1409.1556*, 2014.
- [67] R. J. Williams, “Simple statistical gradient-following algorithms for connectionist reinforcement learning,” *Machine Learning*, vol. 8, pp. 229–256, 1992.
- [68] T. Chen, M. Li, Y. Li, M. Lin, N. Wang, M. Wang, T. Xiao, B. Xu, C. Zhang, and Z. Zhang, “Mxnet: A flexible and efficient machine learning library for heterogeneous distributed systems,” *arXiv preprint arXiv:1512.01274*, 2015.
- [69] R. R. Selvaraju, M. Cogswell, A. Das, R. Vedantam, D. Parikh, and D. Batra, “Grad-cam: Visual explanations from deep networks via gradient-based localization,” in *Proceedings of the IEEE International Conference on Computer Vision*, 2017, pp. 618–626.
- [70] R. Likert, “A technique for the measurement of attitudes,” *Archives of Psychology*, 1932.